

Prediction of Astrometric Microlensing Events during the Gaia Mission

Svea Profit, Markus Demleitner, and Joachim Wambsganss

Astronomisches Rechen-Institut, Zentrum für Astronomie der Universität Heidelberg, Mönchhofstraße 12-14, 69120 Heidelberg, Germany

Received 8 July 2011 / Accepted 30 September 2011

Abstract

We identify stars with large proper motions that are potential candidates for the astrometric microlensing effect during the Gaia mission i.e. between 2012 and 2019. The effect allows a precise measurement of the mass of a single star that is acting as a lens. We construct a candidate list by combining information from several input catalogs including PPMXL, LSPM, PPMX, OGLEBG, and UCAC3. The selection of the microlensing candidates includes the verification of their proper motions as well as the calculation of the centroid shift of the source resulting from the astrometric microlensing effect. The assembled microlensing catalog comprises 1118 candidates for the years 2012 to 2019. Our analysis demonstrates that 96% of the (high) proper motions of these candidates are erroneous. We are thus left with 43 confirmed candidates for astrometric microlensing during the expected Gaia mission. For most of them the light centroid shift is below $\sim 100 \mu\text{as}$ (assuming a dark lens) or the astrometric deviation is considerably reduced by the brightness of the lens. Due to this the astrometric microlensing effect can potentially be measured for 9 candidates that have a centroid shift between 100 and $4000 \mu\text{as}$. For 2 of these astrometric microlensing candidates we predict a strong centroid shift of about 1000 and $4000 \mu\text{as}$, respectively, that should be observable over a period of a few months up to a few years with the Gaia mission.

Key words. astrometry - high proper motion stars - gravitational lensing

1. Introduction

In the last three decades, gravitational lensing has become an important tool in astronomy and cosmology (Schneider et al. 2006). It is used e.g. to study the mass distribution of galaxies and clusters, to define the large scale geometry of the universe from the determination of the Hubble constant, to discover distant quasars (Blandford & Narayan 1992) or to detect extrasolar planets (Mao & Paczynski 1991). The effect of gravitational lensing is the deflection and magnification of light from a background source by an intervening massive object. For the special case of stellar lenses and sources (Microlensing) there exist two images of the source. If observer, lens and source are perfectly aligned the image will be a ring with angular Einstein radius

$$\theta_E = \sqrt{\frac{4GM_L}{c^2} \frac{D_L - D_S}{D_L D_S}}, \quad (1)$$

where M_L is the mass of the lens and D_S , D_L are the distances of the source and the lens to the observer (Chwolson 1924; Einstein 1936; Paczynski 1986). Typical values of the Einstein radius for Milky Way stars within one kpc distance as lens and distant sources are in the area of a few mas. If the components of gravitational lensing are closely, but not perfectly aligned the two images have an angular separation of order two Einstein radii. Hence it is not possible to resolve the source images with current telescopes. Because the images are not resolvable one can measure only their light centroid. Due to the relative motion of lens, source and observer, the magnification and image geometry changes with time hence the light centroid changes its position as well. The observation of the resulting light centroid shifts of source stars due to gravitational lensing is called astrometric microlensing.

Bohdan Paczynski discussed the interesting possibility to determine the mass of a single star with astrometric microlensing (Paczynski 1995). With this effect it would be possible to determine stellar masses with a precision of about one percent. Except for our sun and a few stars like MACHO-LMC-5 all known geometrically derived stellar masses are obtained from stars who are members of a double or multiple system (Gould et al. 2004). But double stars may not always evolve like single stars. Hence direct measurements of single star masses are very important.

Another very nice feature of astrometric microlensing was emphasized by Paczynski (1995): Astrometric microlensing events can be predicted. For this, one has to identify faint stars with high proper motion. Faint stars are favored because the light centroid shift of the source star is less affected than with a bright lens. High proper motion stars are essential for a short enough time scale. Furthermore these fast moving stars are members of the solar neighborhood which allows the calculation of the lens distances from a parallax measurement with high accuracy. Additionally, the centroid shift is considerably larger for close lenses. Most known high proper motion stars are in a sphere with a radius of about 100 parsec. These stars of the solar vicinity are mainly faint Red Dwarfs.

The first systematic search for nearby astrometric microlensing events was done by Salim & Gould (2000) to identify candidates for the Space Interferometry Mission (SIM). They found 178 candidates during 2005 and 2015 with minimal lens-source angular distances between 7 and 20000 mas. Since then a couple of catalogs with high accuracy in position and proper motion containing faint stars were published, hence it is possible to find more astrometric microlensing candidates, and a calculation of the corresponding centroid shift is more reliable.

With the Gaia mission it will be possible to measure the effect of astrometric microlensing with the required accuracy of order 10 to 100 μas . The satellite, expected to be launched in May 2013, surveys the whole sky and has a lifetime of five years (ESA 2011). It will do astrometry, photometry and spectroscopy of approximately one billion stars in our Galaxy brighter than ≈ 20 mag in the visual band. The Gaia satellite will be the successor of Hipparcos (ESA 1997), the first astrometric satellite. Between 1989 and 1993 Hipparcos measured about one million star positions with unrivaled precision of 1 to 20 mas for stars brighter than 12 mag.

An important quantity for the prediction of microlensing candidates is the astrometric accuracy σ_a of Gaia. It will be ~ 30 to 1400 μas for a single astrometric measurement for stars of brightness 10 to 20 mag (Belokurov & Evans 2002). At the end of the Gaia mission the combined accuracy, which is not relevant for our study, varies between ~ 5 and 200 μas depending on the stellar brightness and the actual number of measurements (de Bruijne 2009). The photometric precision for a single measurement will be ~ 1 to 20 millimag (Varadi et al. 2011; Mignard 2011; Eyer & Figueras 2003) and the photometric accuracy reached at the end of the mission will amount to ~ 0.1 to 2 millimag for stars of brightness 10 to 20 mag (Eyer & Figueras 2003; Perryman et al. 2001; Varadi et al. 2011), respectively.

In this paper we selected astrometric microlensing candidates during the Gaia mission. We explore the possibility that Gaia can measure the resulting centroid shift trajectories.

The paper is structured as follows: In Section 2 we recall the photometric and astrometric signatures of microlensing and the mass determination of the lenses. In Section 3, we present our catalog "Candidates for Astrometric Lensing" and explain its features. In Section 4 we show the candidates for astrometric lensing that have the closest approach between 2012 and 2019 and discuss the candidates that should be observable with Gaia. Finally we summarize the results and give an outlook in Section 5.

2. Basics of Microlensing

2.1. Photometric Microlensing

The magnification due to the focusing of light from a pointlike source by a pointlike lens is called photometric microlensing. The magnification of both source images (A_+ , A_-) and the total magnification A of the light centroid depends only on the impact parameter $u = (\theta_L - \theta_S)/\theta_E$, where θ_L and θ_S are the angular positions of lens and source. The impact parameter is the projected distance between lens and source in units of θ_E . With this the total magnification is represented by Paczynski (1986) as

$$A(u) = |A_+| + |A_-| = \frac{u^2 + 2}{u \sqrt{u^2 + 4}}. \quad (2)$$

The magnification for large impact parameter is approximated by (Dominik & Sahu 2000):

$$\mu(u) \simeq 1 + \frac{2}{(u^2 + 2)^2} \quad (3)$$

and the corresponding magnitude shift by

$$\Delta m = -\frac{5}{\ln 10 \cdot u^4}, \quad (4)$$

i.e. photometric microlensing is measurable only for small values of the impact parameter ($u \lesssim 1$). Hence the timescale of

a photometric microlensing event is typically the Einstein time, the time to cross the Einstein radius, which is expressed by

$$t_E = \frac{D_L \theta_E}{v_\perp} = \frac{\theta_E}{\mu}, \quad (5)$$

where μ is the proper motion and v_\perp the transverse velocity of the lens. From photometric measurements it is possible to derive t_E , but D_L , v_\perp and θ_E (lens mass) can not be extracted individually from observations without additional information.

2.2. Astrometric Microlensing

The astrometric microlensing effect of a close lens with $D_L = 50$ pc and a distant source is illustrated in the upper panel of Figure 1 (following Paczynski 1996a). The lens has an Einstein radius of 8.5 mas and we assume the minimal impact parameter u_0 to be 0.5, which corresponds to a projected distance of 4.25 mas. When a high proper motion star (red crosses) is moving in front of a background source star (big black point) there are two image trajectories due to gravitational lensing (blue open circles). Even if the images are not resolvable one may measure a centroid shift trajectory (violet points) which is always an ellipse. Lens, source, images and the centroid position are all lying on a straight line (dashed line in Figure 1). The black circle presents the corresponding Einstein ring of the event connected with the dashed line. The lower image of Figure 1 shows different centroid trajectories of this astrometric microlensing event. The ellipses correspond to minimal impact parameter of $u_0 = 0.5$ (violet), 1 (blue), $\sqrt{2}$ (red), 2 (green), and 5 (black).

Here we explain the astrometric microlensing signals. First we assume a dark lens. The centroid position is given by Hog et al. (1995), Miyamoto & Yoshii (1995), Walker (1995), and Lee et al. (2010) as

$$\theta_c = \frac{A_+ \theta_+ + A_- \theta_-}{A_+ + A_-}, \quad (6)$$

where θ_+ is the image position outside and θ_- inside of the Einstein ring radius. The light centroid shift in comparison to the unperturbed source position

$$\delta\theta_c = \frac{u}{u^2 + 2} \cdot \theta_E \quad (7)$$

depends on the impact parameter and the Einstein radius. The inner dependence on θ_E is the reason why astrometric microlensing leads to a preference of nearby stars as lenses and distant sources. The corresponding maximal value of centroid shifts is determined by Paczynski (1998) to

$$\delta\theta_{c,\max} \approx 0.354 \theta_E \quad (8)$$

at $u = \sqrt{2}$. For instance, the maximal possible centroid shift of a one solar mass lens at 50 pc and a source at 5 kpc distance amounts to 4.5 mas.

For large impact parameter ($u \gg \sqrt{2}$) one gets a centroid shift of (Dominik & Sahu 2000)

$$\delta\theta_c \simeq \frac{\theta_E}{u}, \quad (9)$$

which implies that the centroid shift decreases only with u^{-1} in comparison to the magnitude shift which depends on u^{-4} . Hence the cross section for astrometric microlensing is much larger than for photometric lensing (Paczynski 1996b; Miralda-Escude 1996).

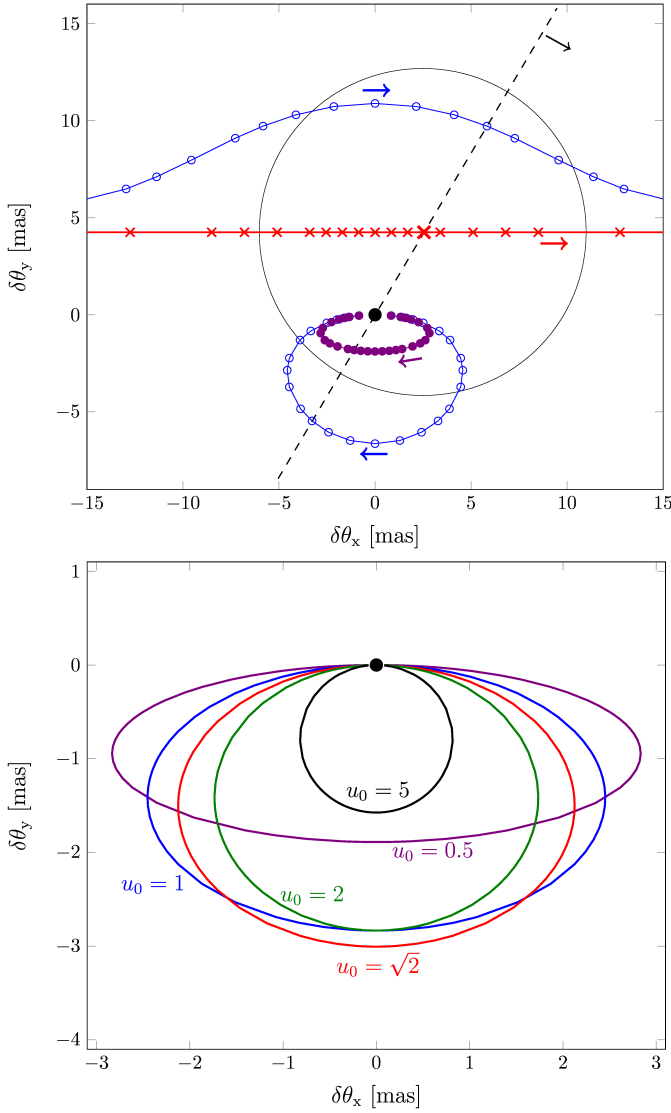


Figure 1. Upper panel: An astrometric microlensing event illustrated with a close lens ($D_L = 50\text{pc}$, $\theta_E = 8.5\text{mas}$) and a distant source (according to Figure 3 of Paczynski 1996a). The lens (red crosses) is moving in front of a background star (big black point) with $u_0 = 0.5$ (equivalent to 4.25 mas). Due to gravitational lensing there are two images whose paths are shown with blue open circles. If the two images are not resolvable one can measure only the light centroid shift trajectory (violet points) which is an ellipse. Lower panel: Different centroid shift trajectories of the same astrometric microlensing event but for different impact parameters $u_0 = 0.5, 1, \sqrt{2}, 2$ and 5 (according to Figure 2 of Dominik & Sahu 2000).

With consideration of the luminous lens effect the centroid position,

$$\theta_{c,\text{lum}} = \frac{A_+ \theta_+ + A_- \theta_- + f_{LS} \theta_L}{A_+ + A_- + f_{LS}}, \quad (10)$$

depends additionally on the flux ratio $f_{LS} = f_L/f_S$ of the lens and the source star. For $u \gg \sqrt{2}$ the centroid shift is reduced by a factor of $1 + f_{LS}$ in comparison to a dark lens (Dominik & Sahu 2000):

$$\delta\theta_{c,\text{lum}} = \frac{1}{(1 + f_{LS})u} \theta_E. \quad (11)$$

If lens and source are both resolved, the luminous lens effect does not need to be considered anymore. The components are resolvable when their projected distance is larger than Gaia's angular resolution, which is about 200 mas .

It is assumed that approximately half of all stars are binaries or multiple systems. In this case the centroid shift ellipse is characterized by distortions, twistings, and jumps (Han et al. 1999). The majority of double stars in the solar neighborhood will be widely separated binary systems. This means they will have a projected binary separation d much larger than the Einstein radius of the primary lens¹. The resulting light curve of this binary system will be very similar to the light curve of the primary lens. But the second lens component can affect the centroid shift trajectory to much larger projected distances (up to $\sim 100 u_0$ depending on the mass of the second lens). For large projected binary separations and a source close to the primary lens the magnification and the centroid shift of the second lens component is approximated to (An & Han 2002)

$$A_2 \sim 1 + 2 \frac{q^2}{d^4} \quad (d \gg 2), \quad (12)$$

$$\delta\theta_2 \sim \theta_{E,1} \frac{q}{d} \quad (d \gg \sqrt{2}), \quad (13)$$

where $q = m_2/m_1$ is the mass ratio of the lens components. The centroid shift of a wide binary lens system can be expressed as the superposition of the individual centroid shifts of both components (Chung et al. 2009):

$$\delta\theta_c \sim \delta\theta_{c,1} + \delta\theta_{c,2}. \quad (14)$$

Due to a larger cross section for astrometric lensing, the duration of astrometric microlensing events is much longer than for the corresponding photometric event. The average duration in which Gaia could measure the astrometric deviation is given by Honma (2001) as

$$t_{\text{ast}} = \frac{\pi}{2} \left(\frac{t_E \theta_E}{\theta_{\min}} \right), \quad (15)$$

where θ_{\min} is the accuracy threshold of Gaia for which the light centroid shift is measurable. We can estimate this threshold to be

$$\theta_{\min} = \frac{3 \sqrt{2} \sigma_a}{\sqrt{5}} \quad (16)$$

where σ_a is the astrometric accuracy of a single measurement, which depends on the source star brightness. The estimation for θ_{\min} is a result of assuming the mean number of consecutive observations to be five (Bastian, priv. comm.), a 3-sigma-area to have a convincing centroid shift measurement, and to get a two-dimensional accuracy (in general Gaia has a high precision in only in one direction) (Belokurov & Evans 2002; Lindegren & Bastian 2011).

The mass of the lensing star can be determined (Paczynski 1998) as

$$M_L = 0.123 M_\odot \frac{\theta_E^2}{\pi_{LS}}, \quad (17)$$

where $\pi_{LS} = \pi_L - \pi_S$ is the parallax of the lens source system. By the use of astrometry it is possible to specify the parallax of at

¹ The primary lens is defined as the binary component with the smallest angular separation to the source.

least the (visible) lensing star. When the lensing star is observable, the angular distance of lens and source is determinable. With additional information of the unaffected source position the centroid shift is measured. With given angular lens-source distance and centroid shift the Einstein radius is calculated by Equation (7). Hence the mass of the lens could be computed by astrometry but the highest accuracy is achieved when the microlensing event is observed both astrometrically and photometrically. Therefore, an accompanying high-cadence ground based photometric monitoring of the events would be advantageous. If the lens is not observable, the combination of photometric and astrometric measurements is necessary. When Gaia will measure two sequenced positional shifts of a source star there will be an alert to do photometric observations from Earth (Wyrzykowski, priv. comm.; Hodgkin & Wyrzykowski 2011). For high proper motion stars it is likely that the time at closest approach, where a photometric event could be observable, has passed by that time. Hence it is important to predict microlensing events in particular for high proper motion lenses.

3. The Microlensing Catalog

3.1. Prediction of Microlensing Events

For the determination of microlensing candidates we search for (background) stars that lie within a certain angular distance to the future position of the high proper motion star as illustrated in Figure 2. The image demonstrates the path of a lensing star between 2008 and 2020 (black arrow). On both sides of the trajectory, a band is defined with a certain minimal angular width w and four corner points. If a source star lies inside this area the lens will be assigned as a candidate for microlensing. In consideration of the positional and proper motion accuracies of the lenses and sources, w was selected to be $0.7''$. Typical accuracies are ~ 100 mas in position and ~ 10 mas/year in proper motion on the standard epoch 2000.0. The increasing width of the trapezium (dashed lines) reflects the increasing uncertainties in the lens position and proper motions as one moves away from this catalog epoch. However, it is sufficient to use the rectangle. Our list "Candidates for Astrometric Lensing" contains the results of this algorithm and can be found at the GAVO data center². It comprises about 2400 microlensing candidates that have their closest approach between 1950 and 2100.

For the prediction of microlensing candidates it was essential to have a reliable catalog of proper motions. The currently most suitable catalog for the sources is the PPMXL (Roeser et al. 2010). It is an all sky catalog with astrometric and photometric information of nearly one billion objects and has a limiting magnitude of ≈ 20 mag in the visual band.

In common astronomical catalogs the majority of stars with high proper motions ($\gtrsim 0.15''/\text{year}$) are spurious. There were many problems with digitalization of old photographic plates, grains on them which were identified as stars, plates from different epochs in different filters or incorrect matching of star positions from different sources especially in regions with high star density. Hence it is difficult to find reliable catalogs for the lensing stars.

Gaia's predecessor Hipparcos produced the Hipparcos and Tycho catalogs which consist of stars brighter than 12 mag. Stars in the solar neighborhood are in general much fainter than this limit. Hence Hipparcos and Tycho contain only few high proper motion stars. Furthermore there exist also some older

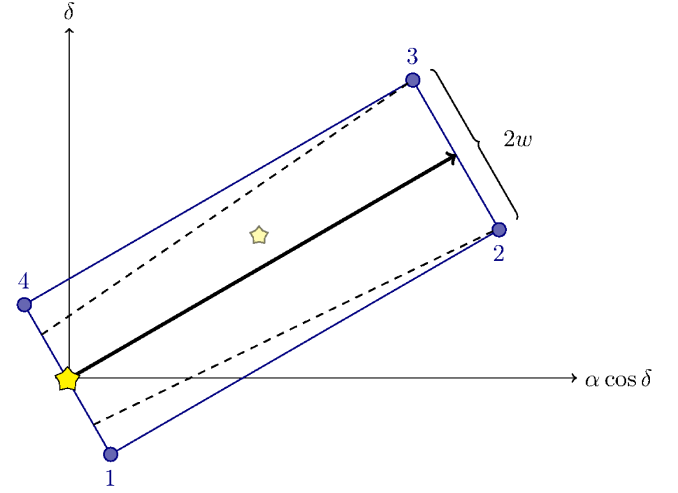


Figure 2. Trajectory of a lensing star in equatorial coordinates between 2008 and 2020 (black arrow). If a background source star (small star) lies inside the area defined with a minimal angular width $2w$ and the corner points 1 to 4, the lens (big star) will be identified as candidate in our table "Candidates for Astrometric Lensing". The rectangle is a simplification of the trapezium (dashed lines), which expresses the increasing uncertainty in the lens positions and proper motions from the catalog epoch 2000.0.

high proper motion star catalogs like NLTT (Luyten & Hughes 1980) or LHS (Luyten 1979), but their positions and proper motions are not precise enough for our study. Considering the limiting magnitude and the positional and proper motion accuracies we selected the LSPM-NORTH (Lepine & Shara 2005), PPMX (Roeser et al. 2008), UCAC3 (Zacharias et al. 2010), and the "catalogue of stellar proper motions in the OGLE-II Galactic bulge fields" (OGLEBG) from Sumi et al. (2004) as lens catalogs. Since the LSPM-NORTH is not available for the whole sky and the PPMX and UCAC3 have not the same quality in every part of the sky they were chosen for different sky regions. The limiting V magnitudes are ≈ 21 mag (LSPM-NORTH), ≈ 15 mag (PPMX) and ≈ 16 mag (UCAC3). Because the probability for microlensing events increases with the density of source stars the majority of microlensing candidates should be close to the Galactic plane. Due to crowding the PPMX, UCAC3, and common proper motion catalogs have a lot of spurious proper motions in sky regions with high star density. Hence we also selected OGLEBG as a lens catalog. OGLEBG contains 5,080,236 stars towards the Galactic bulge with Galactic longitudes $-11^\circ < l < 11^\circ$ and latitudes $-6^\circ < b < 3^\circ$. Of those, about 100 stars have proper motions larger than $0.15''/\text{yr}$.

In the next section we will show that LSPM-NORTH is a suitable lens catalog. It is available only for the northern sky. This catalog contains nearly 62,000 stars with proper motions larger than $0.15''/\text{year}$. The image technique of LSPM-NORTH is different from common proper motion catalogs and leads to correct star identifications and hence to correct proper motions. Another suitable lens catalog is the rNLTT of Salim & Gould (2003). The rNLTT contains about 36,000 stars with declinations larger than -30° . The rNLTT proper motions are with ~ 5.5 mas/year more accurate than the corresponding LSPM-NORTH proper motions (~ 8 mas/year). The rNLTT is the most precise high proper motion catalog with reliable proper motions and comprising faint stars, but it is less complete than LSPM-NORTH in the northern sky, hence we selected the LSPM-

² <http://dc.g-vo.org/aml>

NORTH. We will consider the southern part of the rNLTT as lens catalog in future studies.

Most of our lensing stars are also contained in PPMXL, but occasionally their high proper motion is not listed correctly in this catalog. If the proper motion is known correctly in PPMXL and the proper motion accuracy is better than the considered accuracy of the lens catalog, we used the improved astrometry from PPMXL for the calculation of the centroid shift and the related quantities. The proper motion accuracy of PPMXL varies between 4 and 10 mas/year. The PPMXL mean errors of positions at standard epoch 2000.0 are 80 to 120 mas, when 2MASS astrometry was available (Roeser et al. 2010).

With LSPM-NORTH, PPMX, OGLEBG and UCAC3 as lens catalogs and the PPMXL as source catalogs we find 1118 supposed astrometric microlensing candidates that have their closest approach between 2012 and 2019. Because many of the high proper motions are erroneous we have to individually check the proper motions of all supposed lensing candidates.

3.2. High Proper Motion Analysis

We began the high proper motion analysis with the method of reduced proper motions. This is an important tool to classify star populations (Salim & Gould 2000; Lepine & Shara 2005). By this method a visual magnitude H_V is estimated by use of the proper motion μ . The absolute magnitude is given by

$$M_V = m_V + 5 \log \pi + 5. \quad (18)$$

When the parallax π is replaced by μ , the reduced proper motion magnitude is (Jones 1972)

$$H_V = m_V + 5 \log \mu + 5. \quad (19)$$

Most infrared magnitudes J, H and K are listed in our lens catalogs or are available from 2MASS (Cutri et al. 2003). Hence we can plot a reduced proper motion diagram, i.e. an Hertzsprung-Russell diagram (HRD) with H_V against e.g. J-K. Figure 3 shows this diagram for our 1118 supposed microlensing candidates with known infrared colors in blue triangles and a selection of 10000 Hipparcos stars in red dots. The Hipparcos stars ($V \lesssim 12$) indicate the main sequence and giant branch. Our candidates are all in the area of M-Dwarfs, Subdwarfs or White Dwarfs, but the distribution is much more diffuse than for the Hipparcos stars.

The second proper motion analysis was done with a two color diagram (colors J-H against H-K). The upper panel of Figure 4 shows a two color diagram for 10,000 Hipparcos stars (red dots) and about 200 stars (black triangles) of the "All-Sky Catalog of Bright M Dwarfs" (Lépine & Gaidos 2011). The absolute magnitude of dwarfs and giants increases (fainter stars) from the bottom left to the upper right and the region at $J-H \approx 0.6$ mag is a branch of M-Dwarfs (Bessell & Brett 1988). According to Figure 3, the majority of our 1118 candidates should be in this M-Dwarf branch. The lower panel of Figure 4 shows the same two color diagram but for the selection of Hipparcos stars (red dots) and our microlensing candidates (blue triangles). One can see that the candidates are distributed over all stellar populations. A comparison of the results of the reduced proper motion diagram (Figure 3) and the two color diagram (Figure 4) yields a discrepancy. Because the reduced proper motion diagram (Figure 3) was constructed with the lens proper motions, this discrepancy shows that indeed the majority of lens proper motions are erroneous. Hence we have to check the 1118 microlensing candidates individually to estimate the correct proper motion values.

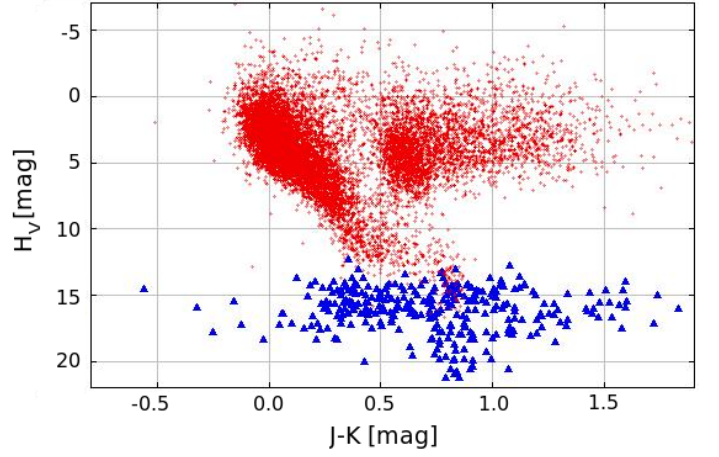


Figure 3. HRD produced with the method of reduced proper motions of the supposed microlensing candidates (blue triangles) and 10000 stars of the Hipparcos catalog (red dots). The magnitude H_V is plotted against the color J-K. According to this plot all lenses should be a M-, Sub- or White Dwarf, but the distribution is very diffuse.

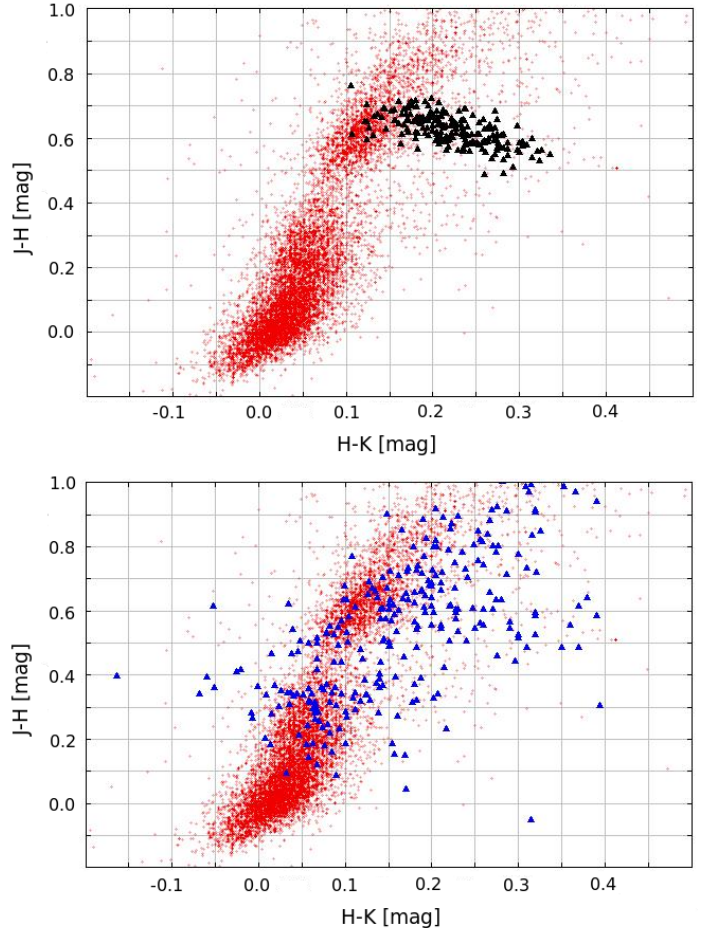


Figure 4. Two-color-diagram to characterize the microlensing candidates. The colors J-H against H-K are shown. In the upper panel 10,000 Hipparcos stars (red dots) and about 200 dwarfs (black triangles) from the "All-Sky Catalog of Bright M Dwarfs" (Lépine & Gaidos 2011) are plotted. The lower panel presents the supposed microlensing candidates (blue triangles) and the same Hipparcos stars as in the upper panel.

The analysis of the lens proper motions was done with the software sky atlas Aladin (Bonnarel et al. 2000). This means we had to “blink” like Lépine & Shara for the generation of the LSPM-NORTH. In order to do that, we chose images from different sky surveys and estimated the lens proper motion. Investigating about 100 lens proper motions, we found that typically the proper motions were correct when the lenses were included in a high proper motion star catalog (like NLTT or LHS). For the remaining supposed candidates it was sufficient to check with SIMBAD (Wenger et al. 2000) which of them are characterized as high proper motion stars.

We found out that 96% of the analyzed 1118 high proper motions are incorrect. Indeed, all LSPM-NORTH proper motions are correct, but most high proper motions from PPMX and UCAC3 were erroneous. We refer to Roeser et al. (2010) for a discussion of a huge number of high proper motion stars in the PPMXL. They pointed out that the majority of them must be wrong based on a comparison to a flat proper motion function between 150 and 430 mas/year.

4. Astrometric Microlensing Candidates

Our list of high proper motion stars as candidates for astrometric microlensing with closest approach to a background source star between 2012 and 2019 comprises 1118 supposed candidates. After double checking the proper motions only 43 actual microlensing candidates remain. Out of those, 36 lensing candidates are on the northern and 7 on the southern sky. The lenses have proper motions between 0.17 and 2.38"/year and apparent magnitudes between 12.1 and 19.9 mag.

When we analyze the reduced proper motion diagram for the actual microlensing candidates (Figure 5) we can see again that our candidate lens stars that have known infrared colors (39 of 43) are all in the regions of Red or White Dwarfs. In comparison to Figure 3, the distribution is very concentrated in a small area. In Figure 6, the two color diagram for the actual microlensing candidates with known infrared colors is shown. In this diagram the remaining candidates (blue triangles) are all located in the Red or White Dwarf branch. Now the comparison of the reduced proper motion diagram (Figure 5) and the two color diagram (Figure 6) of the 39 of 43 microlensing candidates with known infrared colors are in accord.

Our 43 real microlensing candidates are listed in Table 1, ordered by time of closest approach. The table shows the lens ID, the lens and source right ascension and declination at epoch 2000.0, the apparent magnitudes of lens and source, the lens proper motion, the time of closest approach, and the minimal projected distance of lens and source. When we compare these 43 candidates with the 178 candidates from Salim & Gould (2000), who consider a different time interval, we can identify 4 lenses that are contained in both lists. These candidates are our candidate #18 with Salim & Gould #45, #19 with S. & G. #50, #23 with S. & G. #137, and #24 with S. & G. #18. For the 2nd of these candidates the event date is nearly the same (only 20 days difference) and the minimal angular distance only differs by ≈ 180 mas. For the other candidates the event date differs by more than 3 years.

In order to find out which of our 43 candidates are actually detectable with Gaia, a few additional criteria have to be fulfilled:

- The maximal centroid shift has to be larger than the accuracy threshold θ_{\min} of Gaia which depends on the source star brightness.

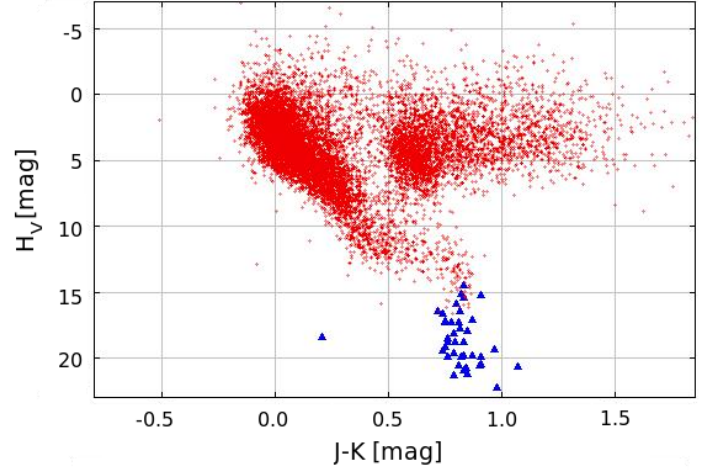


Figure 5. Reduced proper motion diagram of the Hipparcos stars (red dots) and the 39 of our remaining 43 microlensing candidates with known infrared colors (blue triangles). All actual candidates are Red or White Dwarfs

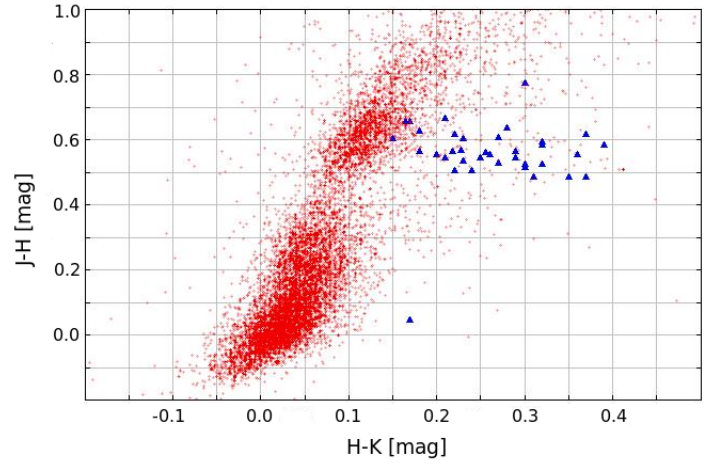


Figure 6. Two color diagram of the Hipparcos stars (red dots) and our 39 real microlensing candidates with known infrared colors (blue triangles). All candidates are in the Red- or White Dwarf branch.

- The astrometric event duration should be at least a few weeks depending on the time interval of observations with Gaia. On average, every two months there are a few consecutive measurements of every object within a few hours.
- The source should be a star and not an extended object like a galaxy.

For the calculation of the maximal centroid shift we need to know the minimal projected distance of the involved stars and the angular Einstein radius. We have computed this angular distance and the time at closest approach with the corresponding uncertainties. To determine the Einstein radius we require an estimation of lens mass, lens distance and source distance. 4 of 43 lenses have known trigonometric parallaxes. For the others we had to resort to photometric parallaxes. Therefore we employ given infrared colors and the luminosity class (see Figures 5 and 6) to get the correct spectral type. Thus we could calculate the absolute magnitudes of our candidates. Then the distance is determined by the distance modulus. The calculated lens distances are between 6 and 476 pc. The lens mass is estimated using the

#	lens ID	α_L (deg)	δ_L (deg)	μ_L ("/yr)	$m_{V,L}$ (mag)	α_S (deg)	δ_S (deg)	$m_{V,S}$ (mag)	t_{\min} (yr)	d_{\min} (")
1	UCAC3 206.42273 -51.01684	206.42273	-51.01684	0.527	15.3	206.42335	-51.01857	18.5	2012.11	0.070
2	LSPM J2226+2913	336.73694	29.22514	0.230	13.6	336.73794	29.22537	19.6	2012.26	0.050
3	OGLEBG 737206	270.92908	-28.42642	0.171	15.9	270.92897	-28.42691	19.6	2012.35	0.756
4	LSPM J2205+3730	331.44064	37.50056	0.279	16.7	331.44176	37.50014	19.6	2012.35	0.198
5	OGLEBG 490395	271.39029	-28.19142	0.186	17.6	271.39011	-28.19197	16.2	2012.45	0.125
6	LSPM J2104+5325	316.09170	53.42085	0.221	19.1	316.09250	53.42135	19.8	2012.49	0.148
7	LSPM J0916+0926	139.05100	9.44044	0.212	13.0	139.05022	9.43994	18.9	2012.55	0.386
8	LSPM J0905+6733	136.43961	67.56268	0.862	14.6	136.43501	67.56012	20.7	2012.83	0.405
9	LSPM J1905+6022	286.49097	60.37719	0.240	17.9	286.49023	60.37802	18.4	2012.88	0.046
10	LSPM J1948+3250	297.10131	32.84255	0.215	14.9	297.10186	32.84325	17.0	2012.94	0.129
11	LSPM J0352+3620	58.02211	36.34658	0.156	19.6	58.02267	36.34599	20.6	2012.95	1.504
12	LSPM J1441+1731	220.28276	17.52493	0.228	18.3	220.28340	17.52436	20.8	2012.96	0.496
13	LSPM J0427+7609	66.87036	76.16094	0.342	14.6	66.87380	76.15995	20.1	2013.16	0.234
14	LSPM J1943+0941	295.80650	9.69005	0.507	17.2	295.80546	9.68842	16.1	2013.62	0.675
15	LSPM J0020+0044	5.20582	0.74310	0.207	17.0	5.20656	0.74287	20.3	2013.76	1.268
16	PPMX 130002.0 -284329	195.00840	-28.72489	0.431	14.8	195.00987	-28.72590	19.4	2013.79	0.070
17	LSPM J2111+3123	317.86120	31.38924	0.235	18.1	317.86223	31.38967	19.9	2013.95	0.481
18	LSPM J0431+5858E	67.80238	58.97810	2.375	12.1	67.81246	58.97045	19.7	2014.04	0.133
19	LSPM J0207+4938	31.76613	49.64538	0.486	12.1	31.76761	49.64367	18.7	2014.34	0.061
20	LSPM J2004+3808	301.08704	38.14137	0.341	12.7	301.08606	38.14012	12.7	2014.51	0.037
21	LSPM J2130+4842	322.58025	48.70194	0.260	16.0	322.58137	48.70279	19.2	2014.69	0.490
22	UCAC3 211.75498 -72.81659	211.75498	-72.81659	0.242	14.7	211.75163	-72.81717	19.6	2014.72	0.238
23	LSPM J0730+3248	112.53480	32.80781	0.213	18.3	112.53393	32.80738	17.0	2014.96	0.722
24	LSPM J0225+4227	36.42162	42.45195	0.180	18.2	36.42300	42.45174	17.9	2015.17	1.483
25	LSPM J1356+2858	209.14762	28.98275	0.188	14.7	209.14694	28.98214	20.3	2015.47	1.331
26	LSPM J2035+6453	308.87289	64.89700	0.303	15.0	308.87534	64.89790	19.2	2015.49	1.192
27	LSPM J0218+3731	34.64142	37.51808	0.169	16.3	34.64229	37.51820	20.4	2015.58	0.253
28	LSPM J2022+2657	305.61134	26.95245	0.331	16.3	305.61082	26.95104	19.6	2015.97	0.012
29	LSPM J1625+1540	246.30813	15.68172	1.216	14.2	246.30872	15.67635	20.6	2016.11	0.055
30	LSPM J1020+2915	155.07403	29.25383	0.289	19.1	155.07369	29.25261	18.5	2016.33	0.514
31	LSPM J1330+1909	202.62941	19.15944	1.385	15.2	202.62699	19.15347	20.3	2016.75	0.100
32	LSPM J0301+7310	45.29591	73.16964	0.291	18.8	45.30031	73.16911	19.3	2016.8	0.179
33	UCAC3 226.36393 -46.33785	226.36393	-46.33785	0.530	14.7	226.36077	-46.33899	18.7	2016.9	0.424
34	LSPM J1209+0042	182.36808	0.70392	0.386	14.4	182.36629	0.70379	17.9	2016.95	0.152
35	LSPM J1502+3531	225.54918	35.53155	0.411	19.3	225.54721	35.53039	19.8	2017.28	0.699
36	LSPM J2008+2358	302.11758	23.96755	0.220	18.3	302.11870	23.96806	19.6	2017.42	0.724
37	LSPM J0107+3412	16.94937	34.20847	1.462	12.8	16.95775	34.21086	19.7	2017.46	0.485
38	UCAC3 253.86047 -64.54973	253.86047	-64.54973	0.203	15.9	253.85828	-64.55027	18.6	2017.68	0.226
39	LSPM J0646+1304	101.58121	13.07978	0.255	18.1	101.58178	13.07863	18.9	2018.29	0.054
40	LSPM J0729+3308	112.45441	33.14243	0.191	19.0	112.45431	33.14201	19.2	2018.34	1.522
41	LSPM J0228+6553	37.01399	65.89983	0.192	19.3	37.01595	65.89915	20.1	2019.06	0.352
42	LSPM J0633+5257	98.36513	52.96467	0.198	19.9	98.36574	52.96358	20.6	2019.51	0.389
43	LSPM J0450+1704	72.66384	17.08175	0.216	15.1	72.66481	17.08098	16.9	2019.88	0.328

Table 1. The 43 real (out of 1118 supposed) astrometric microlensing candidates between 2012 and 2019. Given are the lens ID, the lens and source coordinates at equinox J2000.0, the apparent magnitudes of lens and source, the lens proper motion, the time at closest approach, and the minimal angular distance of lens and source. 9 of these candidates are printed in boldface and grey background because they could lead to an observable astrometric microlensing event. Detailed information of these 9 expected astrometric microlensing events are given in Table 2.

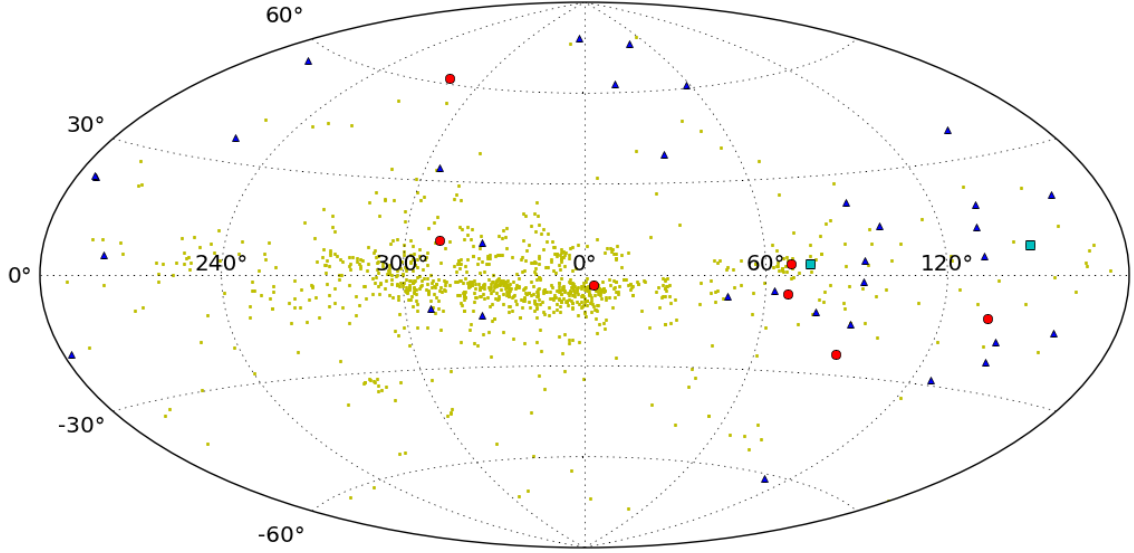


Figure 7. The distribution of all 1118 supposed microlensing candidates. The 1075 spurious candidates (yellow dots), the 43 real candidates (blue triangles, red circles, and green squares) and the 9 best microlensing events (red circles and green squares) are represented in Galactic coordinates (Aitoff projection). The 2 events that should be observable with Gaia are plotted as green squares. The majority of microlensing candidates and possible events are close to the Galactic plane.

spectral type and the luminosity class. For the White Dwarf masses we used the mean value of the mass-distribution from DA-White Dwarfs from the Palomar Green Survey (Liebert et al. 2005), since the majority of White Dwarfs are in this group. The analysis yields that all lens masses are smaller than the mass of the sun (0.08 to 0.6 solar masses).

For the sources, a distance determination was not possible. Hence we had to use an estimation of the Einstein radius for distant sources, which is

$$\theta_E = 0.902 \text{ mas} \sqrt{\frac{M}{M_\odot} \frac{10 \text{ kpc}}{D_L}}. \quad (20)$$

In this way the Einstein radii are estimated to between 2 and 30 mas. The minimal impact parameters of our lensing candidates are ~ 2 to ~ 600 Einstein radii. Assuming a dark lens, we would get maximal centroid shifts of ~ 4 to $\sim 6000 \mu\text{as}$. But when the lens brightness is equal or larger than the source brightness we have to consider this effect. Unfortunately, this is the case for the most candidates at closest approach. Thus we calculated the maximal centroid shift for a luminous lens with the assumption of large impact parameters (equation 11). Besides we determined the centroid shift at the projected lens-source distance of 200 mas (Gaia’s angular resolution) where the luminous lens effect has not to be considered anymore ($\delta\theta_{c,\text{res}}$).

The time interval, for which a large enough astrometric signal is measurable with Gaia, is defined as t_{ast} (equation 15). For our 43 microlensing candidates, this time interval ranges between 3 days and 2525 days.

After analysis of the source characteristics we could identify only one extended source. This source is probably a galaxy and not a pointlike object thus the corresponding lens is not a suitable candidate (#16 in Table 1).

Now we want to identify the best candidates using the above criteria. The study of the maximal centroid shift ($\delta\theta_c$ at u_0 for $u_0 \geq \sqrt{2}$), considering the precision compared to the threshold θ_{min} , yields 9 astrometric microlensing candidates with closest

approach between 2012 and 2019. Due to positional uncertainties, proper motion uncertainties and uncertainties of the estimated masses and distances, the accuracy of the centroid shift has the same order of magnitude as the centroid shift itself for an individual measurement. When we include the luminous lens effect and the above criteria only 2 very good candidates remain that fulfill all required criteria. This means that under ideal conditions it is possible to measure the microlensing effect for 9 candidates with Gaia, but it appears robust only for 2 of them.

The 9 possible astrometric microlensing candidates, their positions and proper motions, and calculated parameters are shown in Table 2, ordered by time of closest approach. In this table the 2 best microlensing candidates are #18 and #20.

The Galactic distribution of all microlensing candidates is shown in Figure 7. The yellow dots represent the 1075 spurious candidates, the other symbols (blue triangles, red circles, green squares) the 43 real microlensing candidates, the red circles and green squares the 9 best candidates, and the green squares the 2 probably measurable microlensing events. Due to a higher density of background stars, the majority of microlensing candidates are close to the Galactic plane. Because of crowding this is also the region with the highest rate of spurious high proper motions and hence the part of the sky that contains most erroneous candidates.

4.1. Excellent Astrometric Microlensing Candidate LSPM J0431+5858E

Now we will give some more information on the 2 best lensing candidates. The first candidate is the White Dwarf LSPM J0431+5858E (also known as GJ 169.1 B, LHS 27 or Stein 2051 B) which is a member of a double star system. The projected binary separation is about $8''$. It is a very widely separated system and hence the effect of the second lens, which has probably only half the mass of the primary, is negligible. With equation (13) it can be seen that the resulting centroid shift of the second compo-

#	1	2	5	10	18	19	20	28	34
lens ID	UCAC3 206.42 273-051.01684	LSPM J2226 +2913	OGLEBG 490395	LSPM J1948 +3250	LSPM J0431 +5858E	LSPM J0207 +4938	LSPM J2004 +3808	LSPM J2022 +2657	LSPM J1209 +0042
t_{\min} (yr)	2012.11±0.97	2012.26±0.65	2012.45±6.39	2012.94±0.66	2014.04±0.08	2014.34±0.33	2014.51±0.60	2015.97±0.56	2016.95±0.36
ϑ_{\min} (")	0.070±0.333	0.050±0.194	0.125±0.468	0.129±0.142	0.133±0.160	0.061±0.130	0.037±0.201	0.012±0.173	0.152±0.137
l (deg)	311.57425	88.69476	2.84945	68.24745	148.10341	135.29101	74.47165	67.22408	280.33137
b (deg)	10.94226	-23.87574	-3.40778	3.63157	7.31408	-11.40291	3.59330	-5.74691	61.72031
μ_L ("/yr)	0.527	0.230	0.186	0.215	2.375	0.486	0.341	0.331	0.386
V_L (mag)	15.3	13.6	17.6	14.9	12.1	12.1	12.7	16.3	14.4
MK	M4 V	M4 V	M4 V	K7 V	DC WD	M3 V	M1 V	M4 V	M3 V
M_V (mag)	11.5	11.5	11.5	8.5	13.3	10.7	9.5	11.5	10.7
M_L (M_{\odot})	0.3	0.3	0.3	0.55	0.6	0.35	0.45	0.3	0.35
D_L (pc)	57.7	26.1	169.3	192.3	5.6	19.3	42.9	92.5	55.7
θ_E (mas)	6.507	9.678	3.797	4.824	29.560	12.141	9.243	5.138	7.149
u_0 (θ_E)	10.7	5.2	32.9	26.7	4.5	5.0	4.0	2.4	21.3
σ_a (μ as)	540	1050	150	230	1100	610	30	1050	380
θ_{\min} (μ as)	1025	1992	285	436	2087	1157	57	1992	721
$\delta\theta_{c,\max}$ (μ as)	597±2764	1733±5801	115±434	180±216	5972±5946	2239±4140	2069±8810	1591±10782	335±343
$\delta\theta_{c,\text{res}}$ (μ as)	211±88	466±193	72±34	116±55	4186±636	732±278	425±153	132±46	255±128
$\delta\theta_{c,\text{lum}}$ (μ as)	30±147	7±29	92±346	22±29	6±8	5±12	1083±6332	93±1368	13±15
t_E (days)	5	15	7	8	5	9	10	6	7
t_{ast} (days)	45	117	156	142	101	150	2525	23	105
μ_S ("/yr)	0.002	0.038	0.029	0.026	0.011	0.007	0.024	0.007	0.010
V_S (mag)	18.5	19.6	16.2	17.0	19.7	18.7	12.7	19.6	17.9

Table 2. List of the best astrometric microlensing candidates with closest approach between 2012 and 2019 that could be observable within the Gaia mission. The numbers are those of Table 1. The boldface candidates 18 and 20 should be easily measurable with Gaia. The following quantities are shown: time of closest approach (t_{\min}), minimal angular distance (ϑ_{\min}), Galactic coordinates of the lens (longitude l , latitude b), proper motions of lens and source (μ_L ; μ_S), apparent magnitudes (V_L ; V_S), lens spectral type (MK), absolute magnitude of the lens (M_V), lens mass (M_L), lens distance (D_L), angular Einstein radius (θ_E), minimal impact parameter (u_0), positional accuracy (σ_a), accuracy threshold for five consecutive observations (θ_{\min}), maximal centroid shift for a dark lens ($\delta\theta_{c,\text{max}}$), maximal centroid shift with luminous lens effect ($\delta\theta_{c,\text{lum}}$), centroid shift at $\vartheta = 200$ mas ($\delta\theta_{c,\text{res}}$), Einstein time (t_E) and astrometric event duration (t_{ast}).

nent would be only $2 \mu\text{as}$. The lens has a distance to the sun of only 5.6 pc and the highest maximal centroid shift (dark lens) of all 43 candidates ($\approx 6000 \mu\text{as}$). The source is very faint (19.7 mag) and the lens is much brighter (12.1 mag) hence we have to consider the luminous lens effect. But when lens and source are resolvable the centroid shift is still $\approx 4200 \mu\text{as}$ ($\theta_{\min} \approx 2100 \mu\text{as}$). The closest approach of lens and source will be on January 2014 (± 1 month). The time t_{ast} , in which Gaia could measure the astrometric deviation for this event, is about 100 (± 22) days. The mean end-of-mission number of Gaia observations is ≈ 80 spread over about 5 years (de Bruijne 2009; Lindegren 2010; Mignard & Lammers 2011), hence Gaia should measure a clear centroid shift signal at a few different epochs.

4.2. Excellent Astrometric Microlensing Candidate LSPM J2004+3808

The second promising lensing candidate is the M-Dwarf LSPM J2004+3808 (G 125-56) in 43 pc distance. Because lens and source have nearly the same magnitude (12.7 mag), the centroid shift trajectory is less affected by the luminous lens effect. The maximal centroid shift would be $\approx 2070 \mu\text{as}$ for a dark lens and is expected to be $\approx 1080 \mu\text{as}$ with consideration of the lens brightness. The accuracy threshold θ_{\min} amounts to only $57 \mu\text{as}$ due to the bright source star. The closest approach of lens and source will be in July 2014 (± 6 months). The calculated possible observing time with Gaia (t_{ast}) is 2490 (± 1275) days hence the event will be measurable over the whole mission (about 80 times).

5. Summary & Outlook

Our goal was to find and characterize high proper motion stars as candidates for astrometric microlensing detectable with Gaia. We selected 43 microlensing candidates which are available in our list "Candidates of Astrometric Lensing". We used the LSPM, UCAC3, PPMX, and OGLEBG as lens catalogs and the PPMXL as source catalog. The LSPM was a very good selection for the lenses but it is only available for the northern sky. The proper motion analysis with Aladin and SIMBAD showed that 1075 of 1118 (96%) supposed candidates have erroneous proper motions, but all LSPM lenses (36) have correctly determined proper motions. It is well known that this is a typical problem of high proper motions in star catalogs.

We have investigated maximal centroid shifts (for dark and luminous lenses), Gaia's accuracy threshold θ_{\min} , the type of source and the average astrometric event duration to determine which of the 43 remaining actual lensing candidates are detectable with Gaia. Our analysis yields 9 astrometric lensing candidates that could be measurable with Gaia. However, for many of them the observability is marginal due to large centroid shift errors and too short event durations. Two of them have a very strong centroid shift and a long event duration and hence they should be detectable, perhaps also with ground based telescopes astrometrically. These 2 candidates should also lead to a photometrically measurable signal of some millimag. With an Einstein time of 4.5 and 9.9 days, this photometric signal is hardly observable with Gaia, but we can monitor them photometrically from the ground. It is not possible to estimate whether the other 7 possible candidates are observable photometrically due to very short photometric event durations, large impact parameters, and large impact parameter uncertainties, i.e. large uncertainties in the magnitude shift (equation 4).

Gaia's data will be used to produce a catalog with very high precise positions, proper motions and magnitudes of about one billion stars and other astronomical objects with visual magnitudes up to 20. This dataset can then be used for an improvement of the microlensing catalog. On this basis one can predict possible lensing events with much higher accuracy than today. These events could be observed astrometrically with interferometry and photometrically. Hence many single star masses in the solar neighborhood will be determined in the not-so-distant future. The proper motion determinations of Gaia will be very precise so that it would not be necessary to verify all proper motions from the predicted lensing candidates.

Acknowledgements. It is a pleasure to thank Mark Taylor for providing the Tool for Operations on Catalogues And Tables TOPCAT (Taylor 2005) which was used to prepare five figures in this paper. Besides we wish to thank the members of the gravitational lensing group at ARI for helpful comments and discussions to our work, Ulrich Bastian and Stefan Jordan for information about the Gaia mission, Siegfried Roeser for information about astronomical catalogs and their problems, and Kailash Sahu for helpful suggestions on the manuscript. We would like to particularly thank the referee, Andy Gould, for very constructive comments which helped to improve the manuscript significantly.

This publication makes use of data products from the Two Micron All Sky Survey, which is a joint project of the University of Massachusetts and the Infrared Processing and Analysis Center/California Institute of Technology, funded by the National Aeronautics and Space Administration and the National Science Foundation.

References

- An, J. H. & Han, C. 2002, *Astrophysical Journal*, 573, 351
- Belokurov, V. & Evans, N. 2002, *Mon. Not. Roy. Astron. Soc.*, 331, 649
- Bessell, M. S. & Brett, J. 1988, *Astronomical Society of the Pacific*, 100, 1134
- Blandford, R. D. & Narayan, R. 1992, *Annual Review of Astronomy and Astrophysics*, 30, 311
- Bonnarel, F. et al. 2000, *Astronomy and Astrophysics Supplement*, 143, 33
- Chung, S. et al. 2009, *Astrophysical Journal*, 695, 1357
- Chwolson, O. 1924, *Astronomische Nachrichten*, 221, 329
- Cutri, R. M. et al. 2003, *The IRSA 2MASS All-Sky Point Source Catalog*, NASA/IPAC Infrared Science Archive, <http://irsa.ipac.caltech.edu/applications/Gator/>
- de Bruijne, J. 2009, *GAIA astrometric performance: summer-2009 status*, Tech. Rep. 1, European Space Agency
- Dominek, M. & Sahu, K. C. 2000, *Astrophysical Journal*, 534, 213
- Einstein, A. 1936, *Science*, 84, 506
- ESA. 1997, *VizieR Online Data Catalog*, 1239
- ESA. 2011, *ESA Science & Technology: GAIA*, <http://sci.esa.int/science-e/www/area/index.cfm?fareaid=26>, from May 25, 2011
- Eyer, L. & Figueras, F. 2003, *GAIA variable stars Work Reference Document*, obswww.unige.ch/~eyer/VSWG/docs/gaia-var-01.3.ps
- Gould, A., Bennett, D. P., & Alves, D. R. 2004, *Astrophysical Journal*, 614, 404
- Han, C., Chun, M., & Chang, K. 1999, *Astrophysical Journal*, 526, 405
- Hodgkin, S. & Wyrzykowski, L. 2011, *Gaia Photometric (and Astrometric) Science Alerts*, www.ast.cam.ac.uk/~wyrzykow/GAIA/GSAW2011/Talks/hodgkin.pdf
- Hog, E. et al. 1995, *Astronomy and Astrophysics*, 294, 287
- Honma, M. 2001, *Publications of the Astronomical Society of Japan*, 53, 233
- Jones, E. M. 1972, *Astrophysical Journal*, 177, 245
- Lee, C.-H. et al. 2010, *Monthly Notices of the Royal Astronomical Society*, 407, 1597
- Lépine, S. & Gaidos, E. 2011, *The Astronomical Journal*, 142, 138
- Lépine, S. & Shara, M. M. 2005, *The Astronomical Journal*, 129, 1483
- Liebert, J., Bergeron, P., & Holberg, J. 2005, *Astrophysical Journal Supplement Series*, 156, 47
- Lindegren, L. 2010, in *IAU Symposium*, Vol. 261, *IAU Symposium*, ed. S. A. Klioner, P. K. Seidelmann, & M. H. Soffel, 296–305
- Lindegren, L. & Bastian, U. 2011, in *EAS Publications Series*, Vol. 45, *EAS Publications Series*, 109–114
- Luyten, W. J. 1979, *LHS catalogue. A catalogue of stars with proper motions exceeding 0".5 annually*, ed. Luyten, W. J.
- Luyten, W. J. & Hughes, H. S. 1980, *Sep. print University of Minnesota*, Minneapolis, MN (USA), 16 p., 55, 1
- Mao, S. & Paczynski, B. 1991, *Astrophysical Journal Letters*, 374, L37
- Mignard, F. 2011, in *Proceedings of Gaia Follow-up Network for Solar System Objects : Workshop held at IMCCE-Paris Observatory*, ed. I. de Mécanique

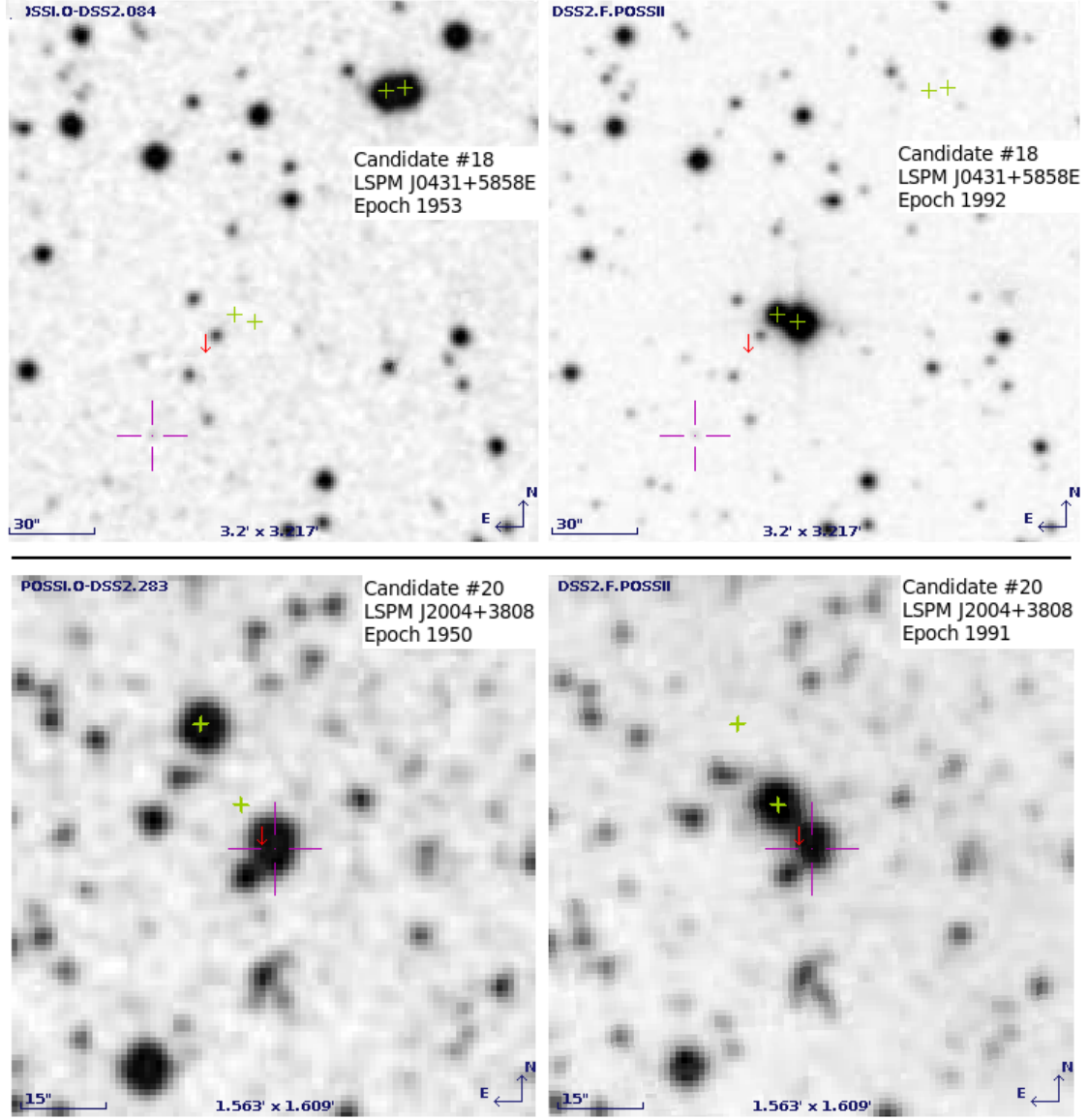


Figure 8. Images from the POSSI and POSSII survey for the 2 best astrometric microlensing candidates produced with Aladin. The upper two figures show the lens candidate LSPM J0431+5858E (candidate #18). The lens candidate is a White Dwarf with an estimated mass of $0.6M_{\odot}$ in 5.6 pc distance and it is a member of a double star system. The two pairs of green plus symbols indicate the double system in the years 1953 and 1992 (the left star is our lens) and the red arrow presents the calculated lens position at the epoch 2000.0. On the bottom panels one can see the second best lensing candidate LSPM J2004+3808 (candidate #20) which has a distance of about 43 pc to the sun. The lens positions in the years 1950 and 1991 are also marked with green plus symbols as well as its position at 2000 is marked with a red arrow. In all images the source star is denoted with a purple cross. One can see that the proper motions of the 2 lensing candidates are correctly given in the LSPM-NORTH catalog.

- Céleste et de Calcul des Ephémérides (IMCCE), Vol. 1 vol., Paris, France, 149 p., 5 p.
- Mignard, F. & Lammers, U. 2011, in EAS Publications Series, Vol. 45, EAS Publications Series, 97–102
- Miralda-Escude, J. 1996, *Astrophysical Journal Letters*, 470, L113+
- Miyamoto, M. & Yoshii, Y. 1995, *Astronomical Journal*, 110, 1427
- Paczynski, B. 1986, *Astrophysical Journal*, 304, 1
- Paczynski, B. 1995, *Acta Astron.*, 45, 345
- Paczynski, B. 1996a, *Gravitational Microlensing in the Local Group*, Tech. Rep. POPe-661
- Paczynski, B. 1996b, *Acta Astronomica*, 46, 291
- Paczynski, B. 1998, *Astrophysical Journal Letters*, 494, L23
- Perryman, M. et al. 2001, *Astron. Astrophys.*, 369, 339
- Roeser, S., Demleitner, M., & Schilbach, E. 2010, *The Astronomical Journal*, 139, 2440
- Roeser, S. et al. 2008, *Astronomy and Astrophysics*, 488, 401
- Salim, S. & Gould, A. 2000, *Astrophysical Journal*, 539, 241
- Salim, S. & Gould, A. 2003, *Astrophysical Journal*, 582, 1011
- Schneider, P., Kochanek, C. S., & Wambsganss, J. 2006, *Gravitational Lensing: Strong, Weak and Micro* (Springer-Verlag)
- Sumi, T. et al. 2004, *Monthly Notices of the Royal Astronomical Society*, 348, 1439
- Taylor, M. B. 2005, in *Astronomical Society of the Pacific Conference Series*, Vol. 347, *Astronomical Data Analysis Software and Systems XIV*, ed. P. Shopbell, M. Britton, & R. Ebert, 29
- Varadi, M. et al. 2011, in EAS Publications Series, Vol. 45, EAS Publications Series, 167–172
- Walker, M. A. 1995, *Astrophysical Journal*, 453, 37
- Wenger, M. et al. 2000, *Astronomy and Astrophysics Supplement*, 143, 9
- Zacharias, N. et al. 2010, *Astronomical Journal*, 139, 2184